JOURNAL OF CONDENSED MATTER NUCLEAR SCIENCE

Experiments and Methods in Cold Fusion

VOLUME 20, October 2016

J. Condensed Matter Nucl. Sci. 20 (2016) 1–225
 ISSN 2227-3123

JOURNAL OF CONDENSED MATTER NUCLEAR SCIENCE

Volume 20 2016

CONTENTS

J. Condensed Matter Nucl. Sci. 20 (2016) 29–53

Research Article

Optical Detection of Phonon Gain Distinguishes an Active Cold Fusion/LANR component

Mitchell R. Swartz*

JET Energy Inc., Wellesley Hills, MA 02148, USA

Abstract

Successful cold fusion is heralded by a large, if not quite abnormal, increase in the anti-Stokes to Stokes (aS/S) ratio in coherent multi-wavelength optical reflection volume-enhanced electric-driven spectroscopy (CMORE-spectroscopy). This distinguishing phonon gain is not seen in the "off" state or the avalanche (undesirable) mode. It heralds seven acoustic phonons assisting nuclear reactions and a core peak calculated Stokes temperature of circa 1645 K.
 ISSN 2227-3123

Keywords: Avalanche mode, CMORE spectroscopy, Excess heat mode, NANOR, Phonon gain

1. Introduction

We previously used dry preloaded NANOR®-type CF/LANR (lattice assisted nuclear reaction) components [1] to investigate material science [2–8] and radiation physics [5,6] of active cold fusion systems. Several of these reports have demonstrated that several electrical transconduction states exist, but that only one is active, desired, and capable of producing "excess heat" [7]. This report extends those results and describes a spectroscopic measurement of anti-Stokes to Stokes (aS/S) peak ratios. These measurements demonstrate that the best "excess heat" results occur (with the CF/LANR nanomaterial in the active, desirable mode) with an aS/S peak ratio greater than 1 (Fig. 1).

Using several ohmic (thermal) and other controls, the aS/S ratio was (and thus acoustic phonons were) found to follow normal Boltzmann statistics when the materials were examined. This included an identical NANOR®-type component which was not loaded, and a similar loaded component in both the "off" condition and electrical avalanche region where the desired cold fusion reactions do not occur. However, that was not true when the cold fusion components are activated in the desired mode which elicits excess heat (Fig. 1). By contrast, the monitored Series 7 NANOR®-type component in "excess heat" (XSH)-mode elicited a completely unique pattern, immediately prior to the appearance of excess heat accumulation. This heralds an aS/S ratio level far above normal, suggesting increased phonon density, consistent with phonon gain. These changes were only seen in the presence of the desired

*Corresponding author. Dr. Mitchell R. Swartz ScD, MD, EE, E-mail: phonongaingroup@nanortech.com.

 ISSN 2227-3123

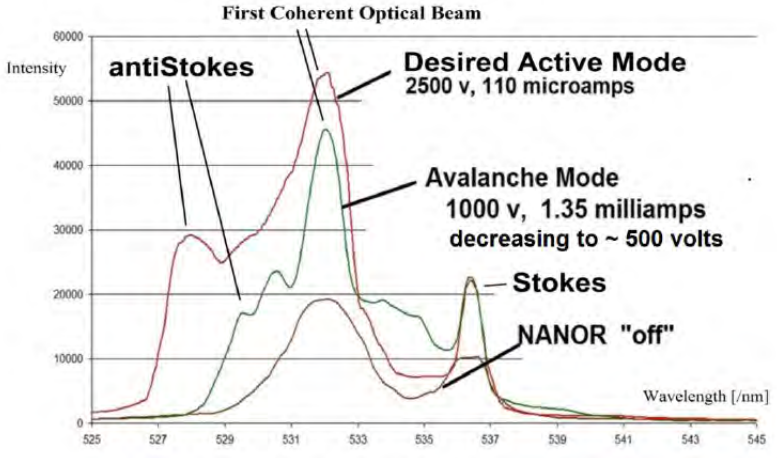

Figure 1. Three different electronic states optical signatures for the same preloaded ZrO_2PdD NANOR®-type CF/LANR component in three different electrical drive modes. Shown are spectra of the same NANOR®-type CF/LANR component in three different electronic states, resolved by dual wavelength coherent electric-driven volume-enhanced reflection spectroscopy. The three modes (responses) are the undriven "off"-state, the unwanted electrical avalanche mode [7], and the optimal operational state, the "Desired Active Mode", where "excess" energy is being released.

electronic state of cold fusion (lattice assisted nuclear reaction; CF/LANR) electrical conduction and activity in the NANOR®-type CF/LANR component.

In Fig. 1, the curves are from dual wavelength coherent electric-driven volume-enhanced reflection spectroscopy of the core CF/LANR nanomaterial inside NANOR® 7-6. The plots show reflected optical intensity as a function of wavelength, initially from two incident coherent optical beams but then reflected by backscatter along with the initial optical beams from the core. They reveal three different types of reflection spectra from the same sample, observed by the same diagnostic.

This paper also briefly discusses the response of the NANOR®-type CF component, loaded but not electrically driven, to a magnetic field intensity. The activity is quite complicated in the presence of it being electrically driven, and is discussed elsewhere [4,8].

There are important implications to these new findings. First, other successful cold fusion systems may also indicate their activity by a large, abnormal increase in the anti-Stokes to Stokes (aS/S) ratio. Second, these findings confirm the role of phonons in CF/LANR (previously observed indirectly [9]), and thought to be mainly optical phonons [10]. Third, acoustic phonons result from, or are required for, a cold fusion process producing energy gain in its "excess heat" (XSH) mode in this system.

2. Background – No Additional Applied Magnetic Fields

2.1. Cold fusion requires considerable engineering

The LANR method which Fleischmann and Pons first taught in March 1989 had problems, including inefficiency and non-reproducibility. This created havoc for those inexperienced in metallurgy, electrochemistry, and physics [11–14]. LANR success is rewarded by "excess heat", which means that the energy producing reactions have generated *de novo* helium into the lattice ($\sim 10^{12}$ for every watt-second [15]) and there were adequate conditions to enable energy transfer to the lattice and then to appear as excess heat [10,16]. There may also be other reactions.

One major problem to achieve successful cold fusion has been the difficulty in achieving high D/Pd loadings above $\sim$0.70 near room temperature, and then maintaining that, sometimes for weeks.

Simply put, the rapid increase in deuterium chemical potential acts to limit further loading, but success requires high loading of $>85\%$ for PdD_x hydrides. In most initial efforts, loading was not even considered. Other problems have included the control of vacancies, adequate incubation time, concomitant flux, inadvertent quenching conditions, and lack of critical control of input power.

Many "negative" results are due to a failure to operate the system at the optimal operating point, which is an optimum peak in the excess heat and power gain curves as a function of input electrical power [12,14]. The optimal operating point reflects the relatively narrow peak (maximum) of the biphasic production rate curve for the products obtained by the desired reactions (heat, helium-4) as a function of input electrical power. The problems with loading, and later with optimal operating point manifolds (OOPs) are why initial efforts to replicate successful LANR were so difficult and failed to show excess heat.

2.2. Dry NANOR®-type CF/LANR preloaded components

NANOR®-type devices have been described in the literature [1–7]. The central core generating the excess heat in the desired state involves ZrO_2PdNiD, ZrO_2PdD, and ZrO_2NiD and similar materials [3,18]. A NANOR®-type component is a hermetically sealed cold fusion/lattice assisted nuclear reactions (CF/LANR) nanomaterial, preloaded with D and arranged as a two-terminal electrical component. They are designed to avoid leakage, enabling stabilization and activation of these materials.

2.3. Determination of activity

The LANR preloaded, stabilized NANOR®-type components are driven by a high voltage circuit up to 3000 V rail voltage. This is the high voltage that can be delivered in any run to either the NANOR or the ohmic control used to thermally calibrate the calorimeter.

Input power is defined as $V \times I$. There is no thermoneutral correction in denominator. Therefore, the observed power is a lower limit. The instantaneous power gain (power amplification factor (non-dimensional)) is defined as $P_{\mathrm{output}}/P_{\mathrm{input}}$.

The energy is calibrated by at least one electrical joule control (ohmic resistor) used frequently, and with time integration for additional validation. The excess energy, when present, is defined as $(P_{\mathrm{output}} - P_{\mathrm{input}}) \times$ time.

Data acquisition is taken from voltage, current, and temperature sensors at multiple sites of the solution, and outside of the cell, and even as a 4-terminal measurement of the NANOR®'s internal electrical conductivity. Data acquisition sampling is at data rates of 0.20–1 Hz, with 16–24^{+} bit resolution; voltage accuracy $0.015^{\pm 0.005}$ V, temperature accuracy <0.6°C). The noise power of the calorimeters have been in the range of a milliwatts (for demonstration systems) to tens of microwatts (for present R&D). The noise power of the Keithley current sources driving the reactions is generally $\sim$10 nW or less.

After driving the component and the control in each run, the power and energy gain for both the component and the ohmic control were separately determined both by approximations such as input-power-normalized delta-T incremental ($\mathrm{d}T/P_{\mathrm{in}}$), and input-power-normalized heat flow (delta-HF/P_{in}), and also directly by semiquantitative calorimetry. In the latter, the amount of output energy is determined from the released heat produced during the temperature rise, and then comparing that to the input energy.

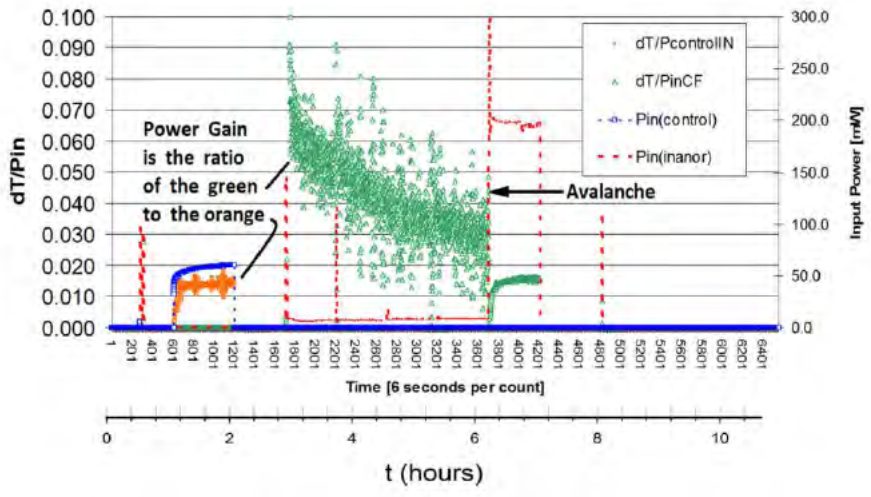

Figure 2. Demonstration of excess power gain and then sudden loss of activity after electrical avalanche for a NANOR®-type LANR component – The electrical input power and delta-T/P in (representative of the measured instantaneous power gain) from the ohmic control and then the nanostructured two-terminal NANOR®-type LANR component. Shown for the component are both sides of the electrical breakdown (avalanche) state; before where there is clear excess power gain (excess heat over time) and a return to ohmic-like behavior at, and after, the electrical avalanche.

2.4. CF/LANR activity quenched by electrical avalanche breakdown

There are two electrically driven states for a driven NANOR®-type LANR component. As described in a series of peer-reviewed publications [7], certain materials of this nature when examined electrically have distinct electrical behavior, with distinct outputs in each of the electrical driven states. To simplify, in addition to the undriven "off" state, there is the undesirable "avalanche" state, which associated with increasing electrical currents for decreasing applied electrical potentials over time. By contrast, the "desired" state produces very large amounts of heat beyond the normal electrical dissipation expected - excess heat. In that case, the electrical impedance is maintained.

Figure 2 presents the graphical output of a reproducible nanostructured NANOR®-type two-terminal CF electrical component, driven in both of its two different electrically driven states; and in its "off" state and also while "off" with an electrical ohmic control being driven. Vertical axes plot the electrical input power and the heat generated, as a function of time.

Figure 2 demonstrates that inactive states exist for "working" CF/LANR components. It shows the measured heat production from the nanostructured two-terminal NANOR®-type LANR component on both sides of the electrical breakdown (avalanche) state; active and quenched. This transformation of active CF/LANR components from active to quenched (inactive states; and there are more than one) is critical to successfully control the desired reactions, and to maximize output, and to avoid damage to some nanomaterials. In the figure, the first curve, extending from count circa 601 to 1201 (where each count is 6 s) is for the ohmic control. The second curve, extending from count circa 1701 to 3701 (where each count is 6 s) is for two-terminal nanostructure component. The electrical input is slowly increased to both the ohmic control and to the component, while each is activated, respectively.

However, only the two-terminal nanostructure component at about count 3701 suddenly undergoes paroxysmal electrical avalanche so that there is simply much more electrical input power as shown in the third curve. It lasts until about count 4201 when the input electrical power is turned off. The first vertical axis, on the left-hand side, represents the heat generated through the parameter $\mathrm{d}T/P_{\mathrm{in}}$ which is the change in temperature elicited, divided by the electrical

input power. Figure 2 plots the temperature rise (delta-T in degrees C) of the ohmic control and the NANOR®-type LANR component, both normalized to input electrical power as a function of time so that the ratios can be used to estimate incremental power gain. By comparing the ratio, a qualitative to semiquantitative estimate of the incremental power gain can be derived, both before electrical avalanche (from the first pair) and after electrical avalanche (from the second pair). Thus, there is obvious incremental power gain for the CF/LANR component until the avalanche, at which time (count ~3700) the component has no energy gain, but has a response similar to an ohmic resistor.

This saliently demonstrates that outside of the desired heat-producing CF/LANR active state, the nanostructured component acts as any other ohmic resistor. Thus, it confirms that the calorimetry was calibrated, and verifies the accurate presence of excess heat yet an additional way. This result also demonstrates significant excess heat obtained from a Ni–D nanomaterial system, as reported previously in a high impedance aqueous CF/LANR system [7,17].

3. Experimental Methods

3.1. CMORE-spectroscopy

Previously, we reported the calibrated near-IR emissions from active aqueous CF/LANR systems [18]. This paper extends that range in nanomaterials to the optic spectrum. The diagnostic, coherent multi-wavelength optical reflection volume-enhanced electric-driven-sample spectroscopy (CMORE-spectroscopy), used for this report required at least two peak wavelengths, usually from two lasers. This was to co-illuminate the real target, located below the irradiated surface, and into the volume, of a sample of interest.

The high intensity coherent illumination was used to elicit Rayleigh, Brillouin, and Raman bands, and then to identify the possible roles of acoustic and optical phonons during CF/LANR, and possibly distinguish the desired active, excess heat-producing, state from the "off"-state, and the undesired inactive avalanche state. Multiple wavelength stimulation was first employed to enable wavelength calibration and thus semiquantitative measurements of the aS/S ratio.

The green laser (532 nm peak) had a power output level of about 150 mW. The orange laser (635 nm peak) had a power output level of about ∼2 mW for energy calibration. Other wavelengths used to calibrate included 436.6 and 546.5 nm peaks of mercury, and the 611.6 nm peak of europium. None was as useful as the second coherent red orange laser.

Laser polarization is usually important to the degree that the nanomaterial is electrically conductive. However, here, the nanomaterial is electrically insulating (∼ megohms to gigohms or more), and is porous, black like bituminous coal. There the light enters and has a volume interaction.

The sample illuminated was the core of a NANOR®-type LANR component capable of being electrically driven. Optics for collimation, control of beam direction, band pass filters, beam splitters, were used to obtain optical beam overlap on the sample's surface, facilitating interaction with the sample while being electrically driven. The important result is that illumination yields many photons which enter the black material which has the appearance of bituminous ground coal (and is ZrO_2–PdD) and react with it. The multifaceted craterous surface leads to a very significant volumetric photon–sample interaction. As a result of the interaction, what was initially just two initial frequencies coming from the two lasers, finally becomes a more complicated spectrum, decorated with the addition of photons of energy both above and below the two frequencies of said lasers.

The Boltzmann aS/S ratio was measured by a method enabling the simultaneous electrical driving of a ZrO_2PdD CF/LANR system in several states while simultaneously visualizing both acoustic and optical phonons using dual wavelength coherent stimulated volume-enhanced Rayleigh–Brillouin–Raman spectroscopy. When the emitted photons have less energy than the initial absorbed photon, then this energy difference is the Stokes shift. The energy goes into the lattice, and the difference is in the "red-shift" direction. On the other hand, if the emitted photon has more energy, the energy gain is called an anti-Stokes shift, and that extra energy is derived from energetic phonons in a

crystal lattice that give up their energy to create the "blue-shift" from the initial two frequencies.

To resolve the spectra (Figs. 3–10), the reflected (exit) beam leaves the illuminated sample through an optical slit and then passes through a diffraction grating where it is resolved into different energies (or in equivalent systems into wavelengths or frequencies). The intensity is measured by a detector such as a CCD or other sensitive photodetector. Analysis is made by integrating the incoming detected optical information which has been sorted by the grating. The

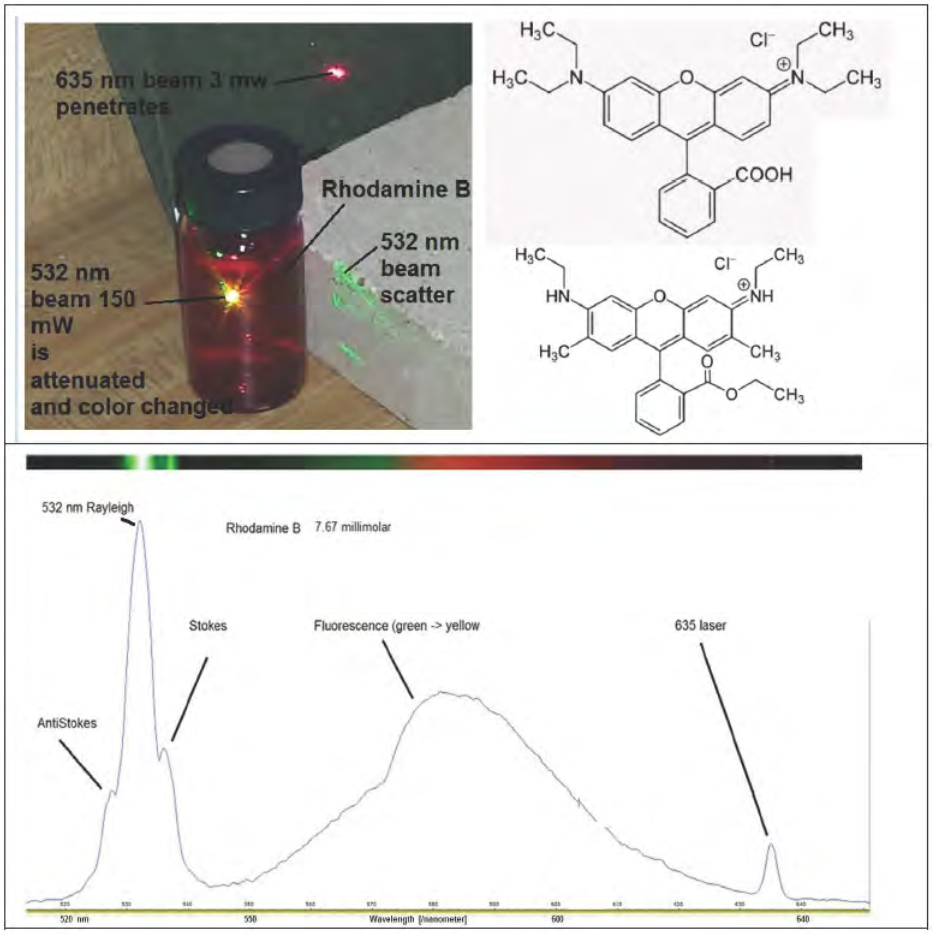

Figure 3. Dual wavelength reflection spectroscopy of a rhodamine B control. (*top-right*) Chemical structure of rhodamine B. Dyes tend to be a range of materials, here varying from (9-(2-carboxyphenyl)-6-diethylamino-3-xanthenylidene)-diethylammonium chloride (above) to the ethyl ester carboxyphenyl methylamino methyl xanthenylidene-ethylammonium chloride (below). (*top-left*) Optical scatter and passage through a small glass container of 7.6 mmol rhodamine B solution. The glass, irradiated by two co-linear lasers (532 and 635 nm) from the lower left (not seen), reveals the green laser only by fluorescence as yellow, although the scatter remains green on the right. Passing through the glass, the orange laser beam continues, exiting on the top right. (*bottom*) This CMORE-spectroscopic spectrum is a control experiment of rhodamine B (7.6 mmol aqueous solution). The vertical axis is non-linear and represents the intensity of the returned backscatter along with the reflected optical information, plotted as intensity as a function of wavelength. The horizontal axis plots the decreasing frequency to the right. The Stokes, anti-Stokes and fluorescence bands are seen in their well-known locations, and the two laser initiation wavelengths (532 and 635 nm) are seen and labeled. The actual image is located above the graph.

final plots show the total energy of the reflected beams in a distribution of amplitude (intensity) as a function of wavelength.

3.2. Electrical driving components

The sample or component was electrical driven, or not, while it was irradiated by the two lasers while physically maintained in position. The NANOR®-type component was electrically activated and controlled, and was designed to include and use several controls: several metals and material controls such as ZrO_2Pd and ZrO_2Ni, pn-junctions (as an energy conversion control), a thermal ohmic control, a non-functional unloaded NANOR®-type component control, an inactive undriven component as a control, an inactive driven avalanche-mode component as a control, and a component driven in the desired active mode.

The electrical power supply is capable of delivering an electric current (Norton equivalent) or electric voltage (Thevenin equivalent) through the two wires which connect to the sample. The system has several electrical states, the simplest of which are "off", meaning that the sample is not electrically driven by the electrical power supply, and "on" where there may be a range of electrical driving levels of electrical power (W). Within the holding container there are temperature detectors, and a heat flow detector, linked to a temperature measurement and analytic unit. This enables thermometry to measure any possible incremental temperature change, and therefore analysis of possible heat output from the sample, itself.

3.3. Rhodamine B control

In order to test the system, and here to show the optical purity of the two lasers as well, dual wavelength reflection spectroscopy was performed on a solution of rhodamine B, as a control. The generated spectrum acts as a control to demonstrate the impact of the system on a rhodamine B aqueous solution of which the Stokes, anti-Stokes, and fluorescence bands are well known.

Figure 3 presents the chemical structure, what a solution of the rhodamine B does to two incoming laser beams, and the resultant spectrum by this system. This control experiment used a 7.6 mmol rhodamine B solution irradiated by the two laser wavelengths (532 and 635 nm). They are labeled in the figure, and the Stokes, anti-Stokes and fluorescence bands are clearly seen, demonstrating the effectiveness of the CMORE-spectroscopic system. The second laser peak permits semiquantitative wavelength (and thus energy) calibration.

4. Results – No Applied Magnetic Field

4.1. ZrO_2Pd – control – unloaded, undriven

As a control, the dual wavelength **r**eflection spectroscopy was used to examine an unloaded, undriven NANOR®-type component (ZrO_2Pd). The results are shown in Fig. 4.

4.2. ZrO_2PdD – control – undriven (null, "off state")

Figure 5 shows the response of the loaded, deuterated material, ZrO_2PdD, in a NANOR-type component to the dual wavelength reflection spectroscopy. This is a loaded, electrically undriven NANOR-type component (ZrO_2PdD). There was no additional electrical activation (as will be seen in some of the following figures).

This figure (like the next two) is also in Fig. 1, where the curves are superimposed as much as possible to summarize the discovery.

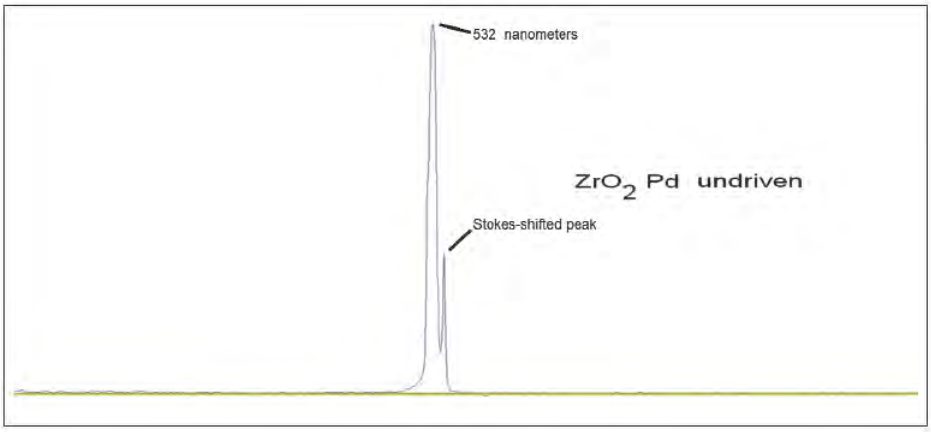

Figure 4. Dual wavelength volume-enhanced reflection spectroscopy of an unloaded, undriven NANOR-type component (ZrO_2Pd). This material is discussed elsewhere [3,17] and does not give excess heat [7]. Here the CMORE-spectroscopy reveals a clear Stokes peak with small, negligible, anti-Stokes component. This is discussed further below.

4.3. ZrO_2PdD-loaded, driven (electrical avalanche state)

Figure 6 shows the avalanche behavior by presenting the dual wavelength electric-driven volume-enhanced reflection spectroscopic signature of a loaded (over)-driven NANOR®-type component (ZrO_2PdD) in its avalanche mode.

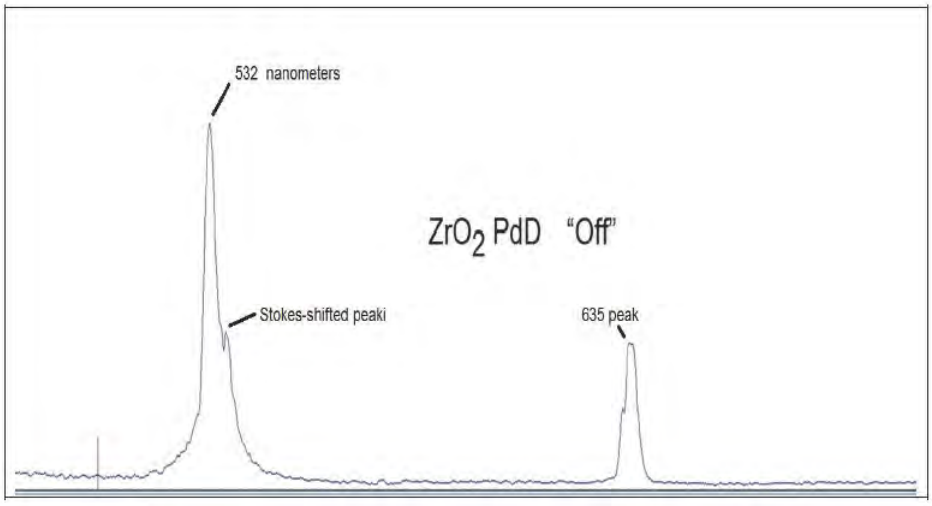

Figure 5. Dual wavelength volume-enhanced reflection spectroscopy of a loaded, undriven NANOR®-type component (ZrO_2PdD). This spectrum is obtained from the NANOR®-type component electrically "Off". Functionally, that makes the observed optical output to be that of the raw material, ZrO_2PdD with no additional electrical drive or activation. The vertical axis represents the intensity of the returned backscatter plotted as intensity as a function of wavelength. The horizontal axis plots the decreasing frequency to the right. The output of the first laser is shown as the peak on the left side, located at 532 nm. The output of the second laser is also shown on the right side, located at 635 nm

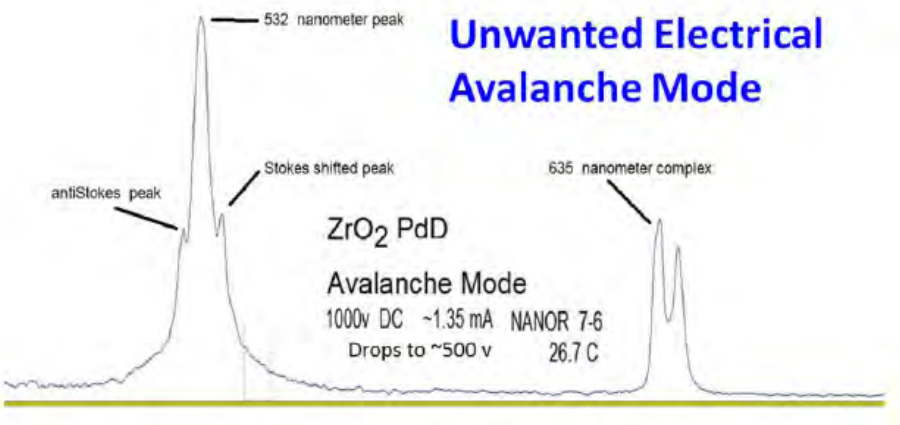

Figure 6. Dual wavelength electric-overdriven volume-enhanced reflection spectroscopy of ZrO_2PdD, a loaded, electrically over-driven NANOR®-type component in avalanche mode – This is the observed optical output in the undesired over-driven avalanche "state" as observed by the diagnostic. The graph, as the others, shows intensity as a function of wavelength of what was returned by backscatter along with the reflected optical beams. There are two groups of peaks. On the left, the peak of the first laser is at 532 nm. In this volume enhanced dual laser backscatter diagnostic, the largest peak is a Rayleigh scattering peak. It can be seen that just to the right of the largest peak is a smaller peak. This peak is almost balanced by a second, slightly smaller peak on the opposite side of the largest peak. These peaks are called Stokes-shifted and anti-Stokes-shifted peaks. What is seen to the left of the tallest peak is termed an anti-Stokes peak. On the right, the second laser interacted with the material and shows its own interactions, making calibration more difficult, so it is usually avoided, but is shown here to demonstrate this effect.

This is the third control "null", in that it is a non-functional (with respect to the desired excess heat) state. However, it is a very high intensity state known as the "Electrical Avalanche" mode, as described elsewhere [7].

This mode, associated with loss of excess heat, was previously presented as a function of time in Fig. 2. For Fig. 6, this loaded nanomaterial, ZrO_2PdD, in a modified two terminal, dry, NANOR®-type LANR electrical component was electrically driven at 1000 V initially (direct current) which enabled a current of about 1.35 mA. Thereafter, the voltage decreased with time to about 500 V. This behavior is what is termed "avalanche mode" and usually results

from excessive applied voltage. The ambient temperature was 26.7°C. Figure 6 shows the observed optical signature during its avalanche "state".

In Fig. 6, the peak of the first laser is at 532 nm; this is the Rayleigh scattering peak. To its right side is a smaller, Stokes-shifted, peak. This is almost balanced by a second, slightly smaller, anti-Stokes peak on the opposite, left side of the largest peak.

Intensity is shown as a function of wavelength, as returned by backscatter along with the reflected optical beams. There is a second peak far to the right, near 635 nm, from the orange laser. In this figure, the second beam was aligned to interact with the reaction volume. Thus, there is more than one single peak. There is a second group of two peaks, located far to the right, near 635 nm, which arise from the orange laser overlap interactions. Usually, the second laser is kept from interacting, and is used as a calibration signal. Here, a rich material science field of energy hopping and conversion are seen, which will be resolved in future efforts.

4.4. ZrO_2PdD-loaded, driven (desired, excess heat state)

The NANOR®-type LANR component is representative of driven CF/LANR systems, in that they are associated with two distinct outputs; one is rather conventional like an ohmic resistor, however, the other state is the electrical "desired" state. That desired mode is characterized by excess heat generation here, and in some experiments involving aqueous D_2O/Pd systems has shown to be linked, in a commensurate way, with the formation of *de novo* ^{4}He [15].

The functional, desired excess heat state of a correctly driven NANOR®-type component (ZrO_2PdD) in its "XSH" mode is non-thermally optically revealed in Fig. 7. The figure shows that the desired CF/LANR activity is indicated by a unique signature using dual wavelength electric-driven volume-enhanced reflection spectroscopy.

This signature advertises behavior which is called "desired mode" or "excess heat production mode" and only results from proper drive voltage, maintaining high impedance, and avoiding quenching materials and quenching states, as discussed elsewhere [1,3,7] and demonstrated conclusively in this report.

For Fig. 7, the nanomaterial NANOR®-type CF/LANR component was properly, correctly electrically driven at 2500 V which produced an electrical current of about 0.11 mA. The sample maintained its high impedance (compared to that seen during avalanche mode) during the very short run and there was no electrical avalanche quenching the desired reactions.

In Fig. 7, the peak of the first laser is at 532 nm; this is the Rayleigh scattering peak. To its right side is a smaller, Stokes-shifted, peak. This is over-balanced by a second, much larger, anti-Stokes peak on the opposite, left side of the largest peak. Note closely that in the best, most preferred, heat producing mode, the so-called "desired state", there is a much larger-than-expected anti-Stokes peak. This is the unique reflected optical output from the desired "excess heat" state where large amounts of energy are being released. Intensity is shown as a function of wavelength, as returned by backscatter along with the reflected optical beams. There is a second peak far to the right, near 635 nm, from the orange laser. The second beam was aligned to not interact with the reaction volume and was only used for calibration. Thus, there is a single peak.

In Fig. 7, the XSH mode can be seen by a unique reflected optical backscatter along with the reflected optical beams from the component in its desired "excess heat" state. Intensity is shown as a function of wavelength, as returned by backscatter along with the reflected optical beams. This is the observed optical output in the desired correctly driven active "state" as observed by the diagnostic. Shown is the output as intensity as a function of wavelength, as returned by backscatter along with the reflected optical beams from the volume-enhanced interactions (*vide infra*). In this run, the second beam did not interact with the reaction volume and was used for calibration. The nanomaterial NANOR®-type CF/LANR component was properly, correctly electrically driven at 2500 V which produced 0.11 mA, and it maintained its high impedance, without electrical avalanche, during the relatively short run.

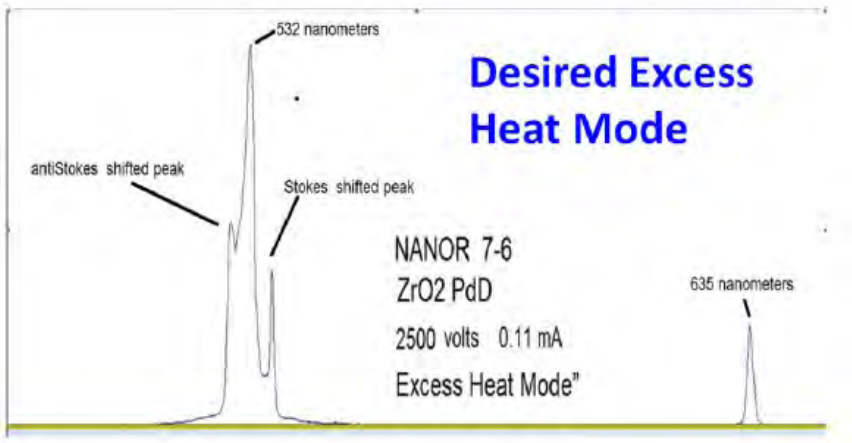

Figure 7. Dual wavelength electric-driven volume-enhanced reflection spectroscopy of a preloaded ZrO_2PdD NANOR®-type component in its correctly driven mode.

4.5. ZrO_2PdD – Optical phonons

In a solid lattice, alloyed with deuterons, there are multiple modes of vibration. The acoustical phonons are those where the palladium and deuterons move in phase in the long wavelength limit, located in reciprocal space at the center of the Brillouin zone. By contrast, optical phonons have from out-of-phase vibrations between neighboring atoms. They are called "optical" because in ionic crystals they can be excited by EM radiation, with the positive ions moving one way while their negatively charged neighbors move the other way. In k (momentum)-space, the phonons appear and manifolds in two branches. The lower manifold contains the acoustical branch, and the higher manifold contains the optical branch. There is an energy gap between them when a single metal is alloyed with hydrogen or deuterium.

To better observe the optical phonons, Fig. 8 is Fig. 7 redrawn, but with a logarithmic vertical axis to enable other peaks, of less intensity, the optical phonons, to stand out. CMORE-spectroscopy resolves and measures all phonon bands, which can be seen at optical frequencies (generally 5–30 THz) and acoustic frequencies (generally 5–15 GHz). The optical phonon bands are not yet well resolved in these first CMORE systems, but the need to do so clearly remains, and explorations should be fruitful.

In Fig. 8, the electrical driving mode of the two-terminal NANOR®-type CF/LANR component is the desired "XSH mode" and only results from proper drive voltage, maintaining high impedance, avoiding quenching materials and quenching states. Importantly, the phonon peaks visualized and measured in the present diagnostic, are both direct evidence of possible optical phonons being involved, and also corroborating the indirect evidence of Cravens et al. [9].

The XSH mode can be visualized by a unique reflected optical backscatter signature. The observed logarithmic optical output in the desired "excess heat" state is returned by backscatter along with the reflected optical beams. Intensity is shown as a function of frequency here to make comparison to the important work of Cravens et al. [9] easier.

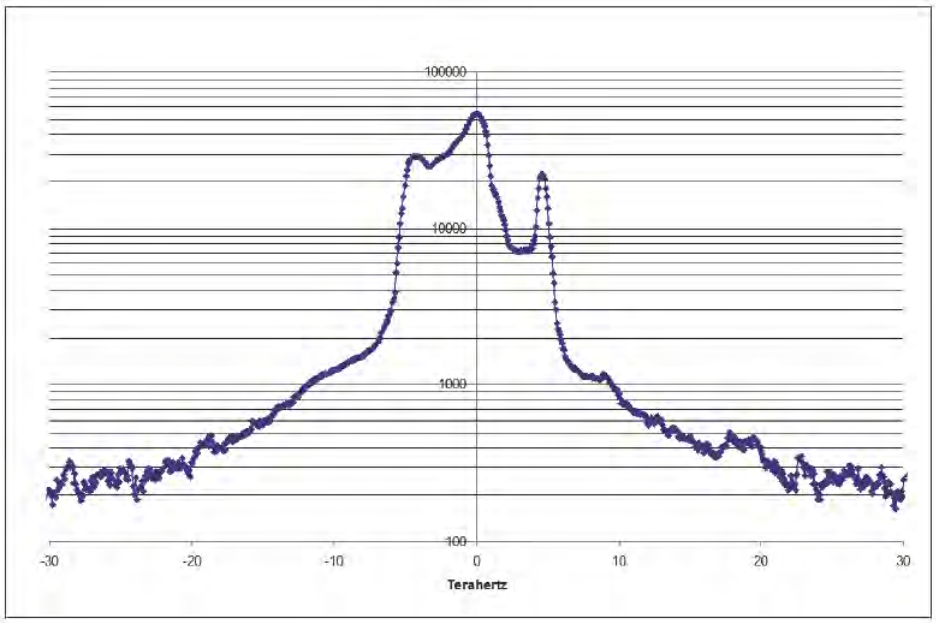

Figure 8. Logarithmic presentation of dual wavelength electric-driven volume-enhanced reflection spectroscopy of a preloaded, correctly driven, ZrO_2PdD NANOR®-type component. The x-axis here presents the frequency difference from the main laser frequency.

5. Results – Magnetic Fields Applied; No Electrical Drive

5.1. Impact of magnetic fields on aqueous CF systems

Previously, magnetic [20–22], and radiofrequency electromagnetic [23] effects have been reported in aqueous cold fusion (a.k.a. lattice assisted nuclear reactions, CF/LANR) systems. In aqueous CF/LANR systems, steady magnetic fields have a small effect which may be inhibitory, especially if perpendicular [22]. In nanomaterial CF/LANR systems, constant magnetic fields produce small effects which may be inhibitory, especially if applied perpendicular to the direction of the applied electric field intensity.

5.2. Impact of magnetic fields on NANOR®-type LANR components

It was discovered that for time varying alternating magnetic interactions with nanostructured CF/LANR systems [4], the post-magnetization effects are significant and time-variant. There is also enhanced improvement of LANR (which occurs at the same time as the magnetization and therefore is called "synchronous").

There are also metachronous effects (occurring later) including power gain and on the observed "heat after death" (HAD); another name for which is the time-integral of the tardive thermal power [12,13], and strong evidence of the first-ever observed two (2) optimal operating point (OOP) manifolds [4].

The application of dH/dt created an increase of 4–10 times the peak power gain over conventional LANR with the same system. The peak power gain of such treated NANOR®s (M-NANOR®s) ranged from 22 to up to ∼80 times input electrical power or more beyond the control, as determined by calorimetry [4]. Furthermore, in contrast to previously observed exponential falloffs of sample activity (peak incremental excess power gain), post-magnetization

activity demonstrates oscillatory activity circa 1.3×10^{-4} Hz (range 0.2-5 $\times 10^{-4}$ Hz). Because of the very complicated issues, magnetically treated NANOR®-type components are called M-NANOR®-type components to distinguish them and anticipate their unique and unusual behavior, and the report here is only of the component in the undriven state with an applied H-field.

There are other impacts of applied magnetic fields intensities on these CF/LANR components. Previously, all CF systems and the NANOR®s have shown a single optimal operating point manifold for excess heat operation, ^{4}He production, and other products. Today, that is no longer accurate. Even after a single treatment to a high intensity Fractionated Magnetic field, there arise two OOP manifolds. The new one is at higher input electrical currents to the NANOR®, and is located to the "right" of the conventional CF/LANR OOP. Thus, magnetically activating preloaded nanostructured CF/LANR devices is very useful [4,18]. Although cold fusion (LANR) has a first stage mediated by phonons within the loaded lattice, there is a magnetically coerced second stage, which we believe may be mediated by magnons, or interactions of phonons in H-field and included magnetization field.

For these very complicated reasons, therefore only the applied H field without activation will be discussed in this initial manuscript.

5.3. ZrO_2PdD "Off" mode, undriven with applied magnetic field

Figure 9 shows the CMORE-spectroscopic signature of the undriven NANOR®-type LANR component (containing ZrO_2PdD) with the simultaneous application of an applied magnetic field of estimated intensity $\sim$2 T. For simplicity, as discussed above, this component was not electrically driven. The electronic vibrations themselves do not produce the desired reactions of excess heat, but with the desired mode they have been demonstrated to produce even more heat [1,3].

Yet, even in the undriven state, it can be observed in Fig. 9, that for this ZrO_2PdD nanomaterial component, the applied high intensity H-field produces an unusual distribution of anti-Stokes electronic vibrations. There is not a single peak like the others, but instead a complex set of H-field induced anti-Stokes peaks. This may be consistent with a distribution of energies or energy level splits as magnetic fields wrought, such as with the Zeeman effect, or as discussed below consistent with inhibiting the effect of the ZrO_2 alone.

5.4. ZrO_2PdD "Off" – width of anti-Stoke peaks and magnetic field

Figure 10 shows the half width of these H-induced distributions of anti-Stokes peaks which appear during the presence of the applied magnetic field. Figure 10 was obtained by three consecutive runs in which the magnet was brought next to, and half way to, the optically irradiated component. It can be seen that the H-induced width of the anti-Stokes peaks increases, but that the increase appears to plateau in this most qualitative of experiments.

In Fig. 9, at 105.6/cm, the calculated Boltzmann statistics ratio is 0.60. The Boltzmann intensity ratio was actually 0.32. At 56/cm, the calculated Boltzmann statistics ratio is 0.76. The Boltzmann intensity ratio was actually 0.51. Both are qualitatively close.

This curve, shown as intensity as a function of wavelength, was returned by backscatter along with the reflected two optical laser beams. Only one laser peak is shown here, with the upper level well beyond the range of the graph; the other peak is far to the right. The units are 1/cm from Raman spectroscopy.

6. Interpretation

6.1. Excellent signal picked up by CMORE spectroscopy

There are many important questions, issues, and ideas that accrue from these studies and observations. They begin with the response itself. The black granular nanomaterials fortunately give very large signals. Why are there such

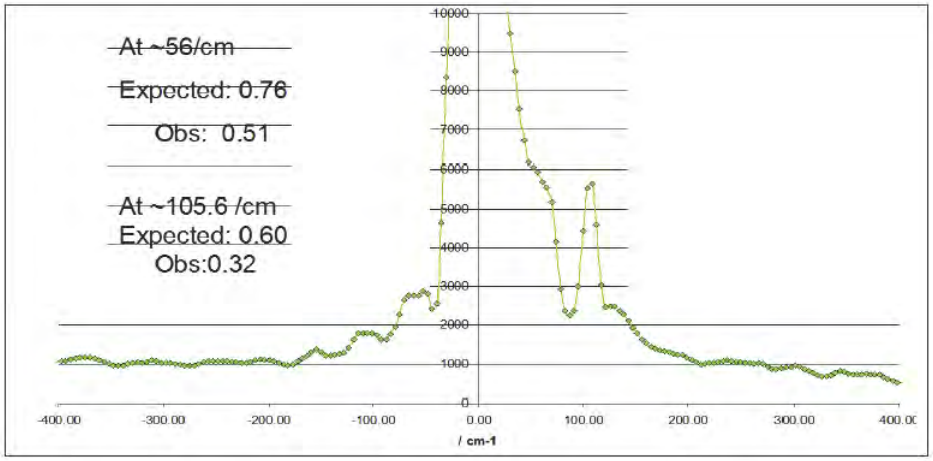

Figure 9. Dual wavelength volume enhanced spectroscopy. The observed optical output of the NANOR®-type LANR component (containing ZrO_2PdD) with no additional electrical drive/activation, the "off" state, but with an additional static applied magnetic field intensity of approximately 2 T at its peak, abutting the core. The x-axis here is plotted as normally done in Raman spectroscopy with the units of (1/cm), to which it is normalized.

large peaks? And, a corollary is: why is there such volume enhancement. The volume enhancement is probably from the black nanostructured CF/LANR materials which are black, electrically insulating, and therefore will accept light deeply into the material, very unlike a conductive metal electrode.

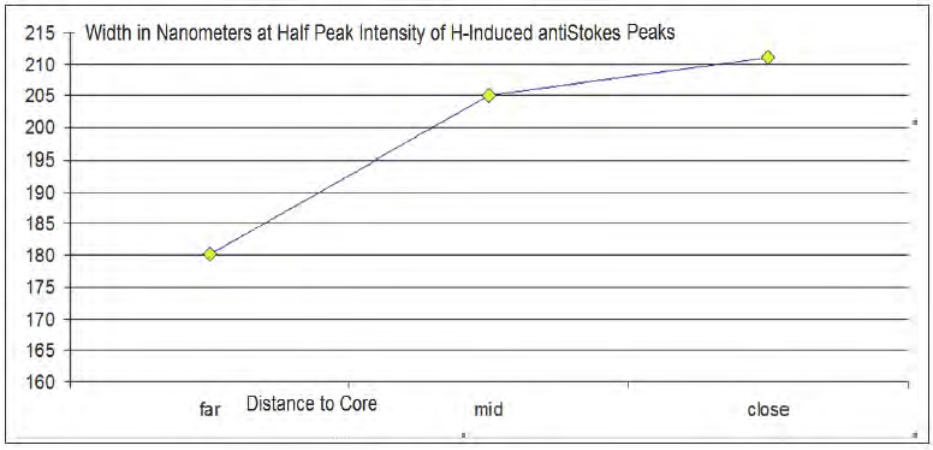

Figure 10. Half width of the newly appearing distribution of anti-Stokes peaks which appeared only with a magnetic field intensity, imaged using dual wavelength electric-driven volume enhanced (CMORE) spectroscopy. Shown is the half intensity width in nanometers in the presence of an applied magnetic field. This figure qualitatively represents three runs in which the magnet was brought successively closer to the surface of the irradiated, undriven, loaded component.

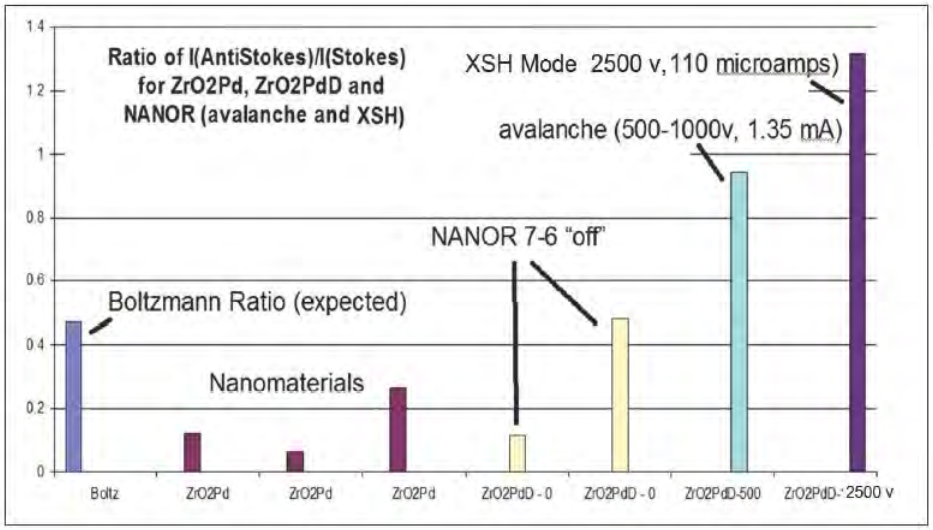

Figure 11. Histogram of measured Boltzmann ratios and what is expected. Shown are the experimental Boltzmann ratios measured for a series of materials, and a NANOR®-type LANR component in its three modes.

6.2. Boltzmann statistic and intensity ratio analysis

Figure 11 is a histogram that presents both the Boltzmann statistic ratio and the Boltzmann aS/S intensity ratios which were experimentally measured by the CMORE-spectroscopy for a series of materials, and a NANOR®-type LANR component in its three electrical modes (states). In Fig 11, the horizontal axis shows and identifies eight different categories of said ZrO_2Pd, ZrO_2PdD nanomaterial, and three electrical drive states, and what is expected normally. The vertical axis shows the amplitude of the theoretical Boltzmann statistic ratio and the experimental Boltzmann aS/S Intensity ratios.

In physics, the calculated Boltzmann statistic ratio (also known as the Boltzmann factor) is derived from the frequency and the temperature. Numerically, it is calculated from the exponential of the ratio of two energies. Those energies are the energy of the difference in energies and the thermal energy (which is the Boltzmann constant times the thermodynamic temperature in Kelvin). This is done because the ratio thus reflects the magnitude of the expected populations of the two states.

When those values are inserted into the conventional formulae, the expected Boltzmann statistic ratio is a number between 0.4 and 0.6, as can be seen in the first column of Fig. 11. The other columns were derived experimentally for this report. The Boltzmann aS/S intensity ratio is derived from the actual measured relative intensities of the anti-Stokes peak divided by the intensity of the Stokes peak. Here, those values were determined by CMORE-spectroscopy. Then, the ratio is derived from the intensity of the anti-Stokes peak divided by the intensity of the Stokes peak. The histogram shows the collected information. It was obtained from the data obtained using measured Boltzmann ratios for a variety of related samples; including the relevant ZrO_2Pd nanomaterial, before heavy hydrogen is added, and after the loading deuterons to a very high level [3], and then with the two-terminal component in several electrical drive states.

6.3. Results for unloaded ZrO_2Pd

The second through fourth columns are different preparations of nanomaterial ZrO_2Pd, itself, without the addition of deuterons (heavy hydrogen). The results shown for these three samples demonstrate that they have Boltzmann ratios which are less than expected. This was surprising because for metals and most materials examined, the aS/S ratio was at the level expected, whereas for these nanomaterials examined, the aS/S ratio was at, or below, the level expected.

Why do they act this way? One hypothesis is the presence of volume polaritons removing the anti-Stokes population by dissipating the energy. A polariton is light bound to an exciton. They are bosonic quasiparticles, different from polarons (which is an electron bound to a group of coherent phonons) which are fermionic. Polaritons are usually considered as surface plasmon polaritons (SPP) which involve infrared through blue electromagnetic waves which travel along a metal–dielectric or metal–air interface. However, here, we propose that the nanomaterial is an electrically insulating (megohms to gigohms or more), volume porous, black (like bituminous coal) absorber. The light enters the volume and has a volume interaction, and some gets reflected back to the surface to be picked up by CMORE spectroscopy.

This volume interaction, through volume plasmon polaritons (VPP) which travel inside the core material, relies on the high impedance dielectric mixed with the island-like widely sequestered highly loaded alloy. VPP would explain the missing anti-Stokes peaks nanomaterials because just as an SPP will evanescently propagate along the surface interface, the VPP will travel further through the volume until its energy is lost.

6.4. Results for loaded undriven ZrO_2Pd

The next two columns were obtained from two samples which were originally from two of the three same nanomaterial samples, except that these two had been very highly loaded with heavy hydrogen. The dry loaded materials were each inserted into a two terminal NANOR®-type CF/LANR component and optically examined. Those samples, not electrically driven, had Boltzmann intensity ratios which ranged from the lowest values up to the normal expected Boltzmann ratio. The upper value for a two-terminal ZrO_2PdD component which was loaded, and "off" with no electric drive, was in the normal range.

The present diagnostic CMORE spectroscopy has revealed the relative absence of anti-Stokes-type peaks in nanostructured materials which are not electrically driven, with the result that the expected Boltzmann ratio is far below what is expected. Why are anti-Stokes-shifted peaks substantively absent for nanomaterials not electrically driven? What is there about nanostructured CF/LANR materials at rest that makes them only dissipate acoustic phonon energy? Probably the multiplicity of available stereoconstellations of the material that allow their dissipation making phonons ephemeral.

6.5. Loaded, avalanche driven ZrO_2PdD

Then, the next columns involve electrical activation: first electrical avalanche, and then the excess heat producing ("desired") mode. When nanostructured NANOR®-type components are driven in Avalanche Mode, the anti-Stokes-type components which appear are different in type, location, and amount, from those which appear during the excess heat producing "desired mode". It has been discovered that there exist increased levels of anti-Stokes-type peaks for all nanostructured materials undergoing electrical drive. Specifically, there is for the avalanche mode for the two-terminal NANOR®-type CF/LANR component close to the near-expected amount of anti-Stokes peaks.

Why the difference? It might be higher in amplitude than the undriven samples in part because the temperature is increased in the sample, and to a lesser degree due in part to second-order curve shift, but the most likely cause is an increase in the acoustic phonon population.

6.6. Loaded, XSH-producing driven ZrO_2PdD

For the activated NANOR®-type CF/LANR component, there was a major, dramatic increase of the anti-Stokes component and the aS/S ratio both greater than expected. It has been discovered that there exist increased levels of anti-Stokes-type peaks for all nanostructured materials undergoing electrical drive, however, the aS/S ratio goes above one only in active, desired mode.

In fact, not only is the anti-Stokes peak of the "desired state" much higher in amplitude than expected for an initial Boltzmann Statistic calculation, it is beyond any known calculated temperature, and beyond what could accrue due to curve shift to a very slight amount.

Figure 11 shows the dramatic increase of the anti-Stokes component for an activated NANOR®-type CF/LANR component. This unusual aS/S ratio exists ONLY with active NANOR®-type LANR component in excess heat producing mode, characterized by a larger electrical impedance which precedes electrical breakdown.

6.7. Magnetic fields in undriven ZrO_2PdD

These magnetic field observations may be quite important. The present diagnostic has discovered that an applied magnetic field of high intensity creates new, multiple low level, distributed anti-Stokes-type peaks which appear for unelectrically driven nanostructured materials.

The increased levels of anti-Stokes-type peaks in correctly driven CF/LANR nanostructured components and materials, and the new lower intensity, but distributed anti-Stokes-type peaks which appear only when a magnetic field intensity is applied, both teach about their role in the coupling of energy production and energy conversion. These new magnetic-induced anti-Stokes-type peaks which appear and indicate a range of energies suddenly having become available (Fig. 9). This may help explain, in part, what applied magnetic fields are doing [4,8], here perhaps working by splitting energy levels like the Zeeman effect [24], thus making them more available.

Another possibility is that the applied magnetic field intensity separates molecular hydrogen into spin isomers. Normally only molecular hydrogen is considered, but another possibility is that it may also separate deuterons within the ZrO_2PdD lattice structure, specifically the local regions interacting where deuterons are held together in a solid solution [25] stereoconstellation with the electrically insulating ZrO_2. This may enable ortho-para states which could influence resonance scattering of phonons by any group of paired or organized clusters of ortho-para deuterons.

7. Conclusions

7.1. Summary of results

The results of measuring $R_{\mathrm{aS/S}}$ in several types of CF/LANR nanomaterials and during different types of electrical activation can be simply summarized in Fig. 11, and in the following Table 1. Figure 11 shows by, histogram of the experimentally measured Boltzmann ratios, and the first column in the histogram shows exactly what is expected by calculation. To the right of that "' expectation" column ("expected"), are shown the experimental Boltzmann ratios actually measured for a series of nanomaterials, and then a NANOR®-type LANR component in its three electrically driven modes.

From Fig. 11, Table 1 compares the information experimentally derived to what was expected by calculation (shown as first column of Fig. 11). The table indicates what was actually experimentally measured compared to those calculated Boltzmann aS/S ratios. In the first two rows, the presence of the lower-energy Stokes-type peaks, and the presence of higher energy anti-Stokes-type peaks are denoted. The final row summarizes how the measured Boltzmann ratios compare to the expected and calculated.

For the first column, the results are for nanostructured material not electrically driven, and therefore is in the "off" state. The second column denotes the result of the application of a very large magnetic fields intensity in the "off"

Table 1. Summary results Boltzmann Stokes ratios: measured versus calculated. The ratio of the actual measured Boltzmann Stokes ratio (Intensity of anti-Stoke-type peak to the Stoke-type peak) as compared to the expected calculated Boltzmann statistic ratios for ZrO_2PdD in a NANOR-type component. The columns represent variants of electric field (E-) drive and H-applied state (not all categories are present).

	Undriven	H-field no E-field	Avalanche E-field	XSH E-field
Stokes	+	+	+	+/-
Anti-Stokes	0/–	–/+	+	+++
I(aS)/(S)	$\ll$ BRatio(calc)	$<$ BRatio(calc)	$\sim$ BRatio(calc)	$\gg$ BRatio(calc)

state. The last two columns denote the results of the loaded ZrO_2PdD NANOR®-type component in both its avalanche (non-excess heat-producing) mode and the desired (excess heat-producing) mode.

7.2. Phonons have been visualized

Previously, cold fusion investigators have not been able to directly see phonons in their hydrogen loaded systems, although they have been inferred indirectly through beat frequency two wavelength systems [9]. By contrast, this new diagnostic enables direct visualization of the actual phonon states of the hydrogen loaded material, even while it is being electrically driven. Specifically, volume-enhanced electrically driven multiwavelength optical (CMORE) spectroscopy decodes cold fusion as it images acoustic and optical phonon prevalence and their diversity.

This preliminary effort has resolved the phonon bands directly in several metals and other materials, and has shown the impact of magnetic fields, of the zirconia itself, of the loading, and of the impact of electrical activation – including the obvious existence of two (2) states (desired XSH and electrical avalanche).

Several questions arise, such as: what are the implications of the separate characterizations of these similar materials? These are important for at least three reasons. First, the phonon gain represent CF/LANR activity, precedes the excess heat, and as has been stated, "LANR and cold fusion have been treated as a "ghost", as there was no way to see the desired state (short of measuring the accrued excess heat later), but this method enables the "ghost" to be seen [26]. This can impact CF/LANR R&D in general, and education and acceptance, as well.

Second, the present CMORE-spectroscopic system reveals that not all CF/LANR nanomaterial states are the same. Note that the active, driven CF/LANR state is not similar to other states or other materials – and it is now distinguishable.

Third, it also reveals that not all electric drive regimes of such CF/LANR systems are the same optically, consistent with thermal and electrical reports [7].

7.3. Acoustic phonon gain during XSH mode

The present diagnostic has revealed new direct evidence of the crucial role of acoustic phonons when a NANOR®-type CF/LANR component is driven in its XSH mode. Specifically, CMORE spectroscopy has revealed a greater-than-normal intensity of anti-Stokes peaks (Figs. 6–11), and therefore acoustic phonon density, only during XSH heat mode compared to both the "off" state and compared to the avalanche mode.

CF/LANR activity is now absolutely linked with acoustic phonons - and only the lattice enables them. Therefore, there are some implications. First, acoustic phonon gain either results from, or is required for, a cold fusion process which produces energy gain in XSH mode. Successful cold fusion creates an aS/S ratio greater than 1 during excess heat. Attention is directed to the fact that in the desired electric-driven excess heat-producing mode, characterized by very high electrical impedance, the two-terminal deuterided NANOR®-type CF/LANR component has a measured Boltzmann Stokes ratio $\sim$1.3.

Second, this discovery is consistent with the role of phonons previously observed indirectly [9], thought to be mainly optical phonons [10]. However, although optical phonons had previously been considered key to the energy transfer of ^{4}He* formed *de novo*, the present diagnostic system has determined a role for acoustic phonons in active CF/LANR systems.

Third, in retrospect, this discovery may also be consistent with the fact that only acoustic phonons are used to calculate the thermal conductivity of a material.

Fourth, how do the XSH-generated acoustic phonons enable the creation of, or de-excitation loss of, ^{4}He* (which is the precursor to de novo ^{4}He seen with the excess heat in aqueous systems [15]?) This diagnostic has detected the existence and visualized a large single anti-Stokes peak, heralding phonon gain, which is ONLY associated with active CF/LANR XSH-production.

7.4. Absent anti-Stokes peaks of undriven ZrO_2PdD and ZrO_2Pd

7.4.1. *Anti-Stokes peaks of undriven ZrO_2PdD and ZrO_2Pd are missing*

Why are the anti-Stokes peaks missing in CF/LANR nanomaterials in ZrO_2?

As discussed above, and seen in Fig. 12, there is significant loss of anti-Stokes peaks in the CF/LANR nanomaterials by this spectroscopy. Where did the anti-Stokes peaks go in the depth of the nanomaterials? The key to understanding that arises from the use of another control, which is ZrO_2, alone. Pure zirconia's CMORE signature is shown in Fig. 12 where the two laser initiation wavelengths of 532 and 635 nm are obvious. However, note that the first peak has a very extended array of Stokes peaks observed falling to its right, in an intensity-decreasing sequence. This optical signature of pure zirconia is unique of all the materials so far examined. ZrO_2 has a thick richness of Stokes peaks. As a control, a white ceramic crucible shows the purity of the laser beam and the absence of the intensity-decreasing pattern of ZrO_2.

This very unusual pattern for ZrO_2 might explain exactly where the anti-Stokes peaks of nanomaterial ZrO_2Pd and

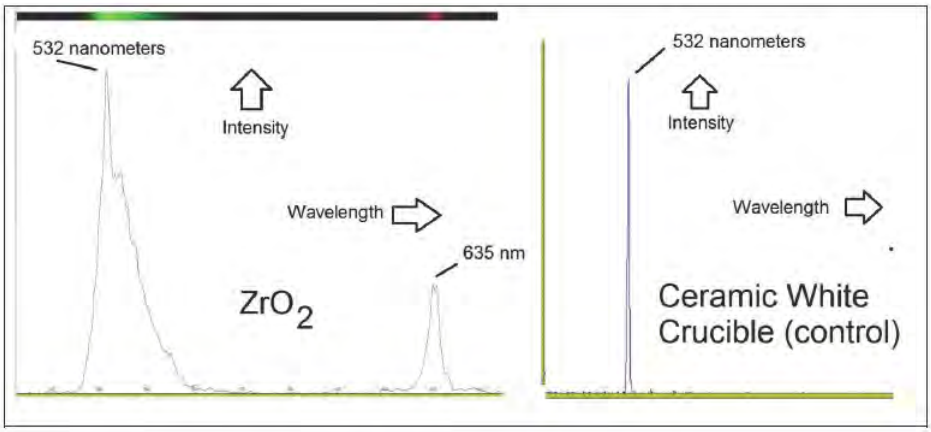

Figure 12. Dual wavelength reflection CMORE Spectroscopy of ceramic control and ZrO_2. (*left*) This CMORE-spectroscopic spectrum is a control experiment of a polished spherical surface of zirconia (ZrO_2) without any other added material. The horizontal axis plots the increasing wavelength to the right. The extended multi-peak Stokes sequence of zirconia is unique for all materials so far examined by this system. The two laser initiation wavelengths (532 and 635 nm) are seen. The actual reflected image is located above the graph. (*right*) As a control, a ceramic white crucible demonstrates the relative purity of the beam, and the absence of the decreasing Stokes peaks that occur with ZrO_2.

ZrO_2PdD disappear prior to electrical activation. Given that Stokes peaks herald loss of energy of incident surface irradiation, it certainly seems possible that ZrO_2 is a molecular system able to dissipate energy through phonons (Fig. 12).

The molecular engineering of ZrO_2PdD thus implies an energy-dissipating cohort of intra-lattice phonons in ZrO_2 under normal conditions prior to electrical activation. What material science stereoconstellation might possibly be the origin of this?

7.4.2. *ZrO_2 unit cell features seven Zr atoms and a vacancy*

The material science must explain why ZrO_2 has the unique feature of an extended array of multiple Stokes peaks in an intensity-decreasing sequence, as shown in Fig. 12. It's unit cell may explain the unique spectrum. Zirconium dioxide (ZrO_2, or "zirconia" from the Persian word "zargun" meaning "gold-colored") is a monoclinic crystal characterized by low thermal conductivity, low electronic conductivity, high tensile strength and a band gap of 5–7 eV. The color may result from the array of optical phonons available (Fig. 12), and be consistent with the observation shown in that figure that ZrO_2 has successive Stokes peaks. However, the acoustic phonon peaks, which are features of Fig. 12, may result because the unit cell of the lattice of ZrO_2 is unlike all the others, such as TiO_2. TiO_2 has a body-centered tetragonal unit cell, with eight titanium atoms in the eight corners. But unlike TiO_2, in ZrO_2 (zirconia), the zirconium eight atoms cannot all fit in the unit cell's corner positions. Instead of eight, because of size and electrostatic considerations, only seven Zr nuclei can fit. As a result, there is a vacancy; and that empty site may be very important for cold fusion (perhaps the very location where cold fusion occurs, driven by the in-phase acoustic phonons). Functionally, the vacancy must be unstable enabling large numbers of vibrations, as revealed in Fig. 12.

7.5. Avalanche anti-Stokes peaks differ from excess heat peaks

The avalanche mode-induced anti-Stokes peaks differ considerably from those observed in the XSH mode, and anti-Stokes peaks are relatively missing in the undriven mode. The avalanche anti-Stokes peaks are greater in number, energy variation, and in lower amounts than the XSH mode-produced anti-Stokes peak.

So one must consider in what way(s) are the XSH-generated acoustic phonons an alternative to the avalanche-generated acoustic phonons for electrical energy dissipation and transfer through the ZrO_2, which acts as an electrical insulator? There appear to be two electrical heat-generating mechanisms which both dissipate energy (both applied and possibly generated internally), and they are distinguished by two entirely different end products, amounts of output heat production, and CMORE signatures. In the unwanted mode, the anti-Stokes peaks of the electrical avalanche indicate conventional dissipation including undesirable electronic and lattice vibrations. In contrast, in the desired excess heat-producing mode, the phonon gain heralded by the large anti-Stokes peaks must somehow tie to unlocking the excited ^{4}He* and coupling the energy released to the lattice as whole.

7.6. Magnetic field increases anti-Stokes peaks

The applied magnetic field intensity-induced anti-Stokes peaks are greater in number, energy variation, and in lower amounts than both the avalanche and the XSH mode-produced anti-Stokes peaks. The complex set of applied H-field-induced anti-Stokes peaks has levels which are qualitatively closer to those expected by calculation. One possibility is that the H-field inhibits movement of charged particles in CF/LANR systems [22], and so here the normal effect of ZrO_2 removing the anti-Stokes peaks of nanomaterials is itself inhibited; and so they reappear. Furthermore, note that the applied magnetic field intensity creates a distribution of energy levels, similar to the Zeeman effect [24,28,29].

7.7. Direct new information about CF/LANR excess heat

7.7.1. *Implications of the aS/S ratio >1 during excess heat*

Why is the aS/S ratio so high with XSH mode in ZrO_2PdD?

There are important implications of an XSH-related aS/S ratio greater than one, from/during the desired cold fusion/LANR state. First, it can indicate, and so far is ONLY associated with, the desired electronic state of cold fusion (lattice assisted nuclear reaction; CF/LANR) activity in a NANOR-type CF/LANR component.

Second, that ratio is significant evidence of acoustic phonon gain, which itself is present only while the preloaded NANOR-type component is driven electrically. The highest levels indicate that the active CF/LANR system, confirmed by the CMORE-spectroscopy, is driven properly.

Third, that ratio is far outside of the range expected normally by temperature alone. It passes through a region which is beyond any known calculated temperature [27]. It is a level greater than could be accounted for by a prosaic curve shift secondary to temperature.

7.7.2. *Calculation of effective temperature during excess heat*

The fact that the Boltzmann Stokes ratio is ∼1.3 reveals more about successful cold fusion. Because the Stokes and anti-Stokes energies are derivable, the effective Stokes temperature can be computed from the experimental data to reveal the core temperature during the XSH mode. The next equation derives the calculated Boltzmann Stokes ratio (BRatio(calc) in Table 1, and sometimes called the calculated Boltzmann Statistic ratio). The equation involves temperature, and is

$$R_{\mathrm{aS/S(calculated)}} = Intensity(\text{anti-Stokes})/Intensity(\text{Stokes}) = \exp(-E_{\mathrm{diff}}/(k_{\mathrm{B}} \times T)), \tag{1}$$

where E_{diff} is the energy difference between the two states is 5.96×10^{-21} J and k_{B} is the Boltzmann's constant. The calculated temperature at core is, therefore, ∼1645 K (∼1372°C).

7.7.3. *Implication of cross-over to phonon gain*

Temperature results from the number of states available to a system [24,28,29]. As the Stokes ratio first rises from the unusually low levels of the CF/LANR nanomaterials, the Stokes ratio is less than 1, the energy difference is positive and temperature has a real, physical value which increases. As the Stokes ratio approaches 1, the energy difference approaches zero, and the temperature is determined by l'Hospital's rule. The limit at a Boltzmann Stokes ratio of 1 is infinity; so technically, this suggests a sudden, tunneling, crossing between the two states. Once the system is on the other side, with a Bolzmann ratios >1, which is the heat producing state, the energy difference is negative and temperature again has a real, physical value.

7.7.4. *Calculation of phonon number during excess heat*

How does the desired XSH mode actually create the anti-Stokes components at levels higher than observed for all other material precursor and avalanche mode? The Stokes and anti-Stokes energies are derivable, and therefore the number

Table 2. Variables used in calculation.

R_{s}	the Stokes ratio = Intensity(anti-Stokes)/Intensity(Stokes)
k_{B}	the Boltzmann's constant = 1.38066×10^{-23} J/K
T	Temperature (K)
$E_{\mathrm{diff}} = \Delta E$	Energy difference

of phonons involved during excess heat can be computed. As discussed in solid state texts [28,29], with an acoustic frequency of 4.9 $^{\pm 0.1}$ THz, there are $\sim$7 $^{\pm 0.15}$ phonons involved. The important point is that this is much lower than has ever been expected before in most theoretic analyses of energy transfer, although it was considered from the point of view of a palladium lattice Pd vacancy surround by 6 deuterons [31].

7.8. The XSH-anti-Stokes peaks and CF/LANR material science

Many questions arise.

- Now, given that acoustic phonons are so important to active CF/LANR systems, then how are they actually linked to the material science?
- What are the material science implications of deriving seven (7) acoustic phonons?
- What might be the physical basis and origin of this?

In this case, perhaps the role results from the inability of hydrogen (deuteron or protium) to normally penetrate the ZrO_2 easily (unlike ionic oxygen), because ZrO_2 is a known electrical insulator. Thus, in zirconium oxide nanostructured CF/LANR materials, one would not expect the lightweight hydrogen nuclei to move across it, but instead rather to remain sequestered as an alloy in the group VIII metallic palladium (or nickel, as it is also used) portions of the separated mixture. The hydrogen remains sequestered, yet crushed by the applied electric field intensity, at the boundary between the alloy and the zirconia.

7.9. Phuson theory corroborated

The proof that phonons are involved as a cohort for the excess heat in active cold fusion (LANR) systems supports the PHUSON Theory. The PHUSON theory [16] of coherent energy transfer to the lattice using phonons appears to be corroborated. It explains the massive energy cooperative transfer from the megavoltage energy of the ^{4}He* to the lattice in a coherent de-excitation process which proceeds by way of lossy spin bosons involving phonons [10] and magnons [4,8]. Hagelstein incorporates the optical phonons in his theory. We have shown here that acoustic phonons have an indelible role.

The PHUSON is the quantum of that energy transfer, in a process which is consistent with conventional physics, and where the energy then appears as “excess heat” [1,11]. The PHUSON theory explains why there is a relative absence of strong neutron and gamma ray emissions in CF (LANR). The gamma emission branch from the excited state of ^{4}He* is actually spin-forbidden for both hot and cold fusion [16]. However, at higher hot fusion temperatures the restriction is lifted slightly. This is consistent to what is seen for both hot and cold fusion. Thus, the PHUSON theory correctly describes the relative absence of neutron emissions in CF (LANR). The only nuclear branches available are those whose band gaps are surmountable by the available activation energy (limited by the ambient temperature and incident radiation).

The neutron emission branch is more than 1 MeV above the first excited state (^{4}He*). Hot fusion has large activation energies available (it is ’hot’). LANR/CF is not. In LANR, given the actual much smaller amount of thermal energy, $k_{\mathrm{B}} \times T$, available for cold fusion ($\sim$1/25 eV), absence of adequate activation energy decisively means that that branch is NOT available, as it is for hot fusion. Neutrons are not observed, ^{4}He production is in its stead. The normally important neutron branch is unavailable at “cold” temperatures. Thus, the PHUSON theory incorporates the observed products, and the energy levels, which explains the branching ratios based on, and explained by, thermal issues. It also explains the origin of the excess heat in active cold fusion systems.

7.10. CAM theory corroborated

The rise in Stokes temperature to circa 1645 K supports that catastrophic solubility effects do occur in PdD driven by local temperatures, and is consistent with, and supports, the Catastrophic Active Medium (CAM) theory [30]. The CAM model of CF considers the deuteron solubility in, and the solubility–temperature relationship of, palladium. The CAM hypothesis treats the metal as an active medium capable of rapid desorption of deuterons with recruitment potential of even more deuterons. The CAM theory describes a quasiparticle related to the sudden catastrophic desaturation of highly loaded Pd involving phonons and moving deuterons into vacancies. The model includes two possible positive feedback loops to account for both the bursts and a plethora of termination sequelae, which declare themselves in several material changes. The results of this model was confirmed by Martin Fleischman just after ICCF-4.

7.11. Implications for development and improvement of LANR systems

The present diagnostic generates spectra in real time which are able to illuminate, visualize, and help identify at least three states for a CF/LANR material or component which is potentially active. The system can determine which state the material or component is in, in real time, even as it is electrically driven, and may be able to determine time constants for changes between levels. Most importantly, it can saliently detect the desired reactions just as products begin to appear and accumulate (e.g. heat). Therefore, it has great use because it reveals both the desired, and undesired, reactions and states and may enable better control, and possible detection of other states of operation – and therefore reactions and products.

7.12. Implications for education

The system enables education of CF/LANR systems. Previous CF/LANR systems have not fully convinced educators and scientists of the importance of hydrogen loaded systems. However, this new diagnostic has additional use as an scientific and educational tool for visualizating different states. The advantage may be the immediate telegraphing of the state, rather than having impatient skeptics await the appearance of excess heat.

7.13. Implications for CF/LANR systems

The use of CMORE-spectroscopy has implications for examining substates in material science and metallurgy, cold fusion physics, and in the electrical engineering of CF/LANR systems. This novel electric-driven coherent high intensity volume-enhanced spectroscopy involves the backscatter of two+ wavelengths from a hydrogen loaded nanomaterial. It is capable of semiquantitative calorimetry (discussed elsewhere [1–3]) and is now demonstrated capable of spectroscopically opening new types of controllable-in-real-time materials science, metallurgy, material engineering, electrical engineering, and electrophysics. Other spectroscopies only identify materials, while the present diagnostic reveals the electrical state of the component while continuing the means to electrically drive, control, and monitor that component and state as desired.

Acknowledgments

The author acknowledges and thanks Gayle Verner for her experimental and editorial support, as well as Jeffrey Tolleson for his editorial assistance and very helpful comments. Thanks also goes out to Peter Hagelstein, Florian Metzler, Dennis Cravens, Pamela Mosier Boss, Lawrence P. Forsley, Louis DeChiaro, Dennis Letts, Joshua Gyllinsky, Brian Ahem, and Jeff Driscoll for their help, ideas and suggestions. This effort was supported by JET Energy Inc. NANOR® and PHUSOR® are registered trademarks of JET Energy, Incorporated. NANOR®-technology, and

PHUSOR®-technology, and the technology described here are protected by U.S. Patents D596724, D413659 and several other patents pending.

References

[1] M.R. Swartz, G. Verner, J. Tolleson and P.L. Hagelstein, Dry, preloaded NANOR®-type CF/LANR components, *Current Science* **108**(4) (2015) 595.

[2] M.R. Swartz and P.I. Hagelstein, Demonstration of energy gain from a preloaded ZrO_2–PdD nanostructured CF/LANR quantum electronic device at MIT, *J. Condensed Matter Nucl. Sci.* **13** (2014) 516. www.iscmns.org/CMNS/JCMNS-Vol13.pdf.

[3] M.R. Swartz, G. Verner, J. Tolleson and P.L. Hagelstein, Energy gain from preloaded ZrO_2–PdNi–D Nanostructured CF/LANR quantum electronic components, *J. Condensed Matter Nucl. Sci.* **13** (2014) 528. www.iscmns.org/CMNS/JCMNS-Vol13.pdf.

[4] M.R. Swartz, G. Verner, J. Tolleson, L. Wright, R. Goldbaum, P.L. Hagelstein, Amplification and restoration of energy gain using fractionated magnetic fields on ZrO_2–PdD nanostructured components, *J. Condensed Matter Nucl. Sci.* **15** (2015) 66. www.iscmns.org/CMNS/JCMNS-Vol15.pdf.

[5] M.R. Swartz, Incremental high energy emission from a ZrO_2–PdD nanostructured quantum electronic component CF/LANR, *J. Condensed Matter Nucl. Sci.* **15** (2015) 92. www.iscmns.org/CMNS/JCMNS-Vol15.pdf.

[6] M.R. Swartz, G. Verner et al., Imaging of an active NANOR®-type LANR component using CR-39, *J. Condensed Matter Nucl. Sci.* **15** (2015) 81. www.iscmns.org/CMNS/JCMNS-Vol15.pdf.

[7] M.R. Swartz, P.I. Hagelstein and G. Verner, Impact of electrical avalanche through a ZrO_2–NiD nanostructured CF/LANR component on its incremental excess power gain, *ICCF-19*, Padua, Italy, April 16, 2015.

[8] M.R. Swartz, Oscillating excess power gain and magnetic domains in NANOR®-type CF/LANR component, in preparation.

[9] D. Cravens, D. Letts and P.I. Hagelstein, Progress on two-laser experiments, *Proc. ICCF15*, 2009. http://lenr-canr.org/acrobat/Hagelsteinprogresson.pdf.

[10] P.L. Hagelstein, Current status of the theory and modeling effort on fractionation, *J. Condensed Matter Nucl. Sci.* **19** (2016)1–9.

[11] M.R. Swartz, Survey of the observed excess energy and emissions in lattice assisted nuclear reactions, *J. Scientific Exploration* **23**(4) (2009) 419–436.

[12] M.R. Swartz, Excess power gain using high impedance and codepositional LANR devices monitored by calorimetry, heat flow, and paired stirling engines, *Proc. ICCF14* **1** (2008) 123. ISBN: 978-0-578-06694-3, 123, (2010); www.iscmns.org/iccf14/ProcICCF14a.pdf.

[13] M.R. Swartz and G. Verner, Excess heat from low electrical conductivity heavy water spiral-wound Pd/D_2O/Pt and Pd/D_2O–$PdCl_2$/Pt devices, *Condensed Matter Nuclear Science, Proc.ICCF-10*, World Scientific, New Jersey, ISBN 981-256-564-6, 29-44; 45-54 (2006).

[14] M.R. Swartz, Consistency of the biphasic nature of excess enthalpy in solid state anomalous phenomena with the quasi-1-dimensional model of isotope loading into a material, *Fusion Technol.* **31** (1997) 63–74.

[15] M. Miles, R.A. Hollins, B.F. Bush, J.J. Logowski and R.E. Miles, Correlation of excess power and helium production during D_2O and H_2O electrolysis using palladium cathodes, *J. Electroanal. Chem.* **346** (1993) 99–117.

[16] M.R. Swartz, Phusons in nuclear reactions in solids, *Fusion Technol.* **31** (1997) 228–236.

[17] Y. Arata and Y.C. Zhang, Observation of anomalous heat release and helium-4 production from highly deuterated palladium fine particles, *Jpn. J. Appl. Phys.* **38** (Part 2, No. 7A) (1999) L774–L776.

[18] M.R. Swartz, Deuterium production and light water excess enthalpy experiments using nickel cathodes, *J. New Energy* **1**(3) (1996) 219. www.iscmns.org/FIC/J/JNE1N3.pdf.

[19] M.R. Swartz, G. Verner and A. Weinberg, Non-thermal near-IR emission from high impedance and codeposition LANR devices, *Proc. ICCF14* **1** (2008) 343, D.J. Nagel and M.E. Melich (Eds.), ISBN: 978-0-578-06694-3, 343, (2010). www.iscmns.org/iccf14/ProcICCF14a.pdf.

[20] D. Cravens, Factors affecting success rate of heat generation in CF cells, *Proc. ICCF-4,* Maui, Hawaii, 1993.

[21] S. Szpak, P.A. Mosier-Boss, F.E. Gordon, Further evidence of nuclear reactions in the Pd/D lattice: emission of charged particles, *Naturwissenschaften* **94** (2007) 511–514.

[22] M.R. Swartz, Impact of an applied magnetic field on the electrical impedance of a LANR device, Vol. 4, *JCMNS Proc*., March 2010, New Energy Technology Symposium held at the 239th American Chemical Society in San Francisco, 2011.
[23] J. O'M. Bockris, R. Sundaresan, D. Letts and Z.S. Minevski, Triggering and structural changes in cold fusion electrodes, *Proc. ICCF4*, Maui, Hawaii, 1993.
[24] A.R. von Hippel, *Molecular Science and Molecular Engineering*, MIT Press, Cambridge, 1959.
[25] B.Ya. Gorodilov, Phonon scattering in ortho-para hydrogen solid solutions (role of configurational relaxation), DOI: 10.1063/1.1542498.
[26] G. Verner, Personal communication.
[27] Anonymous referee, Personal communication.
[28] C. Kittel, *Introduction to Solid State Physics*, Wiley, New York, 1976.
[29] N.W. Ashcroft and N.D. Mermin, *Solid State Physics*, Holt, Rinehart and Winston, New York, 1976.
[30] M.R. Swartz, Catastrophic active medium (CAM) theory of cold fusion, *Proc. ICCF4,* Vol. 4, Maui, Hawaii, 1993, p. 255; sponsored by EPRI and the Office of Naval Research. www.lenr-canr.org/acrobat/EPRIproceedingc.pdf.
[31] D. Letts, A method to calculated excess power, *Infinite Energy* **112** (2013) 63.